Two-photon absorption laser induced fluorescence measurement of atomic oxygen density in an atmospheric pressure air plasma jet.

J Conway[1], G S Gogna[1], C Gaman[1] , M M Turner[1] and S Daniels[1].

[1]National Centre for Plasma Science and Technology, Dublin City University, Glasnevin, Dublin-9, Republic of Ireland.

E-mail: jim.conway@dcu.ie

Abstract
Atomic oxygen number density [O] is measured in an air Atmospheric Pressure Plasma Jet (APPJ) using Two-photon Absorption Laser Induced Fluorescence (TALIF). Gas flow is fixed at 8 slpm, the RF power coupled into the plasma jet varied between 5W and 20 W, and the resulting changes in atomic oxygen density measured. Photolysis of molecular oxygen is employed to allow in-situ calibration of the TALIF system. During calibration, O_2 photo-dissociation and two-photon excitation of the resulting oxygen atoms are achieved within the same laser pulse. The atomic oxygen density produced by photolysis is time varying and spatially non-uniform which needs to be corrected for to calibrate the TALIF system for measurement of atomic oxygen density in plasma. Knowledge of the laser pulse intensity I_0(t), wavelength, and focal spot size allows correction factors to be determined using a rate equation model. Atomic oxygen is used for calibration and measurement, so the laser intensity can be increased outside the TALIF quadratic laser power dependence region without affecting the calibration reliability as the laser power dependence will still be the same for both. The atomic O density results obtained are not directly benchmarked against other known density measurement techniques. The results show that the plasma jet atomic oxygen content increases as the RF power coupled into the plasma increases.

1. Introduction

Atmospheric Pressure Plasma Jets are becoming increasing attractive to industry for surface treatment and modification as expensive vacuum systems are not required, resulting in large cost savings compared to traditional low pressure plasma tools. Cold plasma jet systems are used for surface treatment and modification in areas such as the biomedical industry [1 - 3]. Etching and deposition of various films and materials using plasma jets have also been investigated [4, 5]. Traditionally, plasma jet systems use a He gas feed to carry small concentrations of molecular gases such as O_2 into the plasma, where the molecular gas is broken down [6, 7]. For O_2 gas this leads to the production of species such as atomic oxygen (O) and ozone (O_3), so the plasma becomes chemically activated and can interact with and modify surfaces. For atmospheric air, whose main components are N_2, O_2, Ar and CO_2, the plasma chemistry is very complex. Atomic oxygen has been identified as a key radical in many surface treatment processes so knowledge of the atomic oxygen concentration within the plasma plume and its behaviour with variation in plasma parameters such as flow rate, gas composition and power is of interest [8, 9, 10]. Atomic oxygen density has previously been investigated in various plasma jets. The gas flows used were typically helium/O_2 or argon/O_2 admixtures with O_2 content at a few percent (typically less than 4 %) [6, 11, 12, 13]. Atomic oxygen density has also been measured in jets using Ar/air and He/air gas flows with air content of 1- 5 % [7, 14, 15].

Two-photon Absorption Laser Induced Fluorescence (TALIF) is a useful experimental technique that can be used to measure absolute atomic oxygen number density in atmospheric plasmas [11, 16], and in low pressure plasma tools [17]. TALIF experiments designed to measure absolute atomic oxygen density are typically calibrated using a noble gas scheme first proposed by Döbele *et al* [18]. The calibration procedure involves measuring the TALIF signal produced by a known number density of xenon gas and comparing this to the TALIF signal produced by an unknown density of atomic oxygen. However there are problems associated with this technique. One essential requirement is that the laser power dependence of the TALIF signal be the same for both the measurement and

calibration procedures. This is most easily achieved by ensuring the laser operates in the "linear" region, where the TALIF signal varies in a quadratic manner with laser power during both calibration (Xe) and measurement (O). This inevitably necessitates operating the laser at low laser pulse energies (typically 10's – 100's of μJ per pulse). While this method works well at low pressures, at atmospheric pressure strong quenching of the excited state depletes the population in the upper level before emission can occur resulting in significantly reduced TALIF signals that can be problematic to measure [19]. Increasing the laser power to get stronger TALIF signals can take the laser outside the TALIF quadratic region which complicates the analysis as calibration and measurement TALIF signals may no longer have the same laser power dependence. This occurs as O and Xe have different behaviour for saturation processes such as Two-photon Absorption Laser Induced Stimulated Emission (TALISE), ground state depletion, and Resonance Enhanced Multi Photon Ionization (REMPI) that can occur at higher laser powers [20, 21]. Femtosecond TALIF (fs-TALIF) is one approach that can be used to resolving this issue. fs laser pulse widths are shorter than quenching times in atmospheric plasma and so minimize the effect of collisional quenching on the two-photon absorption process during the laser pulse. As a result, high peak-intensity fs laser pulses produce stronger TALIF signals than can be achieved using equivalent intensities in ns pulse laser systems. Schmidt et al recently used fs-TALIF to measure atomic oxygen density using the xenon calibration scheme in a He/O_2 pulsed atmospheric pressure plasma jet system [22]. A further advantage of the fs method is that interference effects on the atomic oxygen TALIF signal resulting from photolysis of oxygen containing molecules are minimized as high laser pulse intensities can be maintained in fs pulses while using smaller pulse energies. As the number of photons in the high intensity fs laser pulse is significantly less than that in an equivalent intensity ns laser pulse, single photon processes such as photo-dissociation are much smaller in the fs system while the high intensity ensures a strong TALIF signal is maintained. This significantly reduces photolytic interference effects on TALIF signals as discussed by Kulatilaka et al [23, 24].

Photolysis, on the other hand, is an alternative method that can be used to calibrate TALIF experiments [25, 26]. One approach involves using two lasers: one to photo-dissociate a molecular gas producing a known number density $[X]_{Cal}$ of the species of interest X, and a second laser to excite $[X]_{Cal}$ producing a TALIF signal. Alternatively, a single laser pulse can be used to photo-dissociate the molecular gas and two-photon excite the resulting atomic calibration species producing a TALIF signal, all within the same laser pulse. In this work, a single laser pulse both photo-dissociates O_2 molecules, and excites the resulting atomic oxygen via two-photon absorption. Dissociation is a fast process (10^{-12} – 10^{-13} s) compared to the nanosecond width of the laser pulse used in these experiments, so oxygen atoms generated by photolysis have ample time to absorb photon-pairs from the laser pulse giving rise to TALIF signals. There are issues that need to be addressed when using photolysis for calibration. The atomic oxygen density produced in bulk plasma, $[O]_{Plasma}$, is essentially spatially uniform in the laser focal zone, and is also invariant with time during the laser pulse, while that produced by photolysis, $[O]_{Photolysis}$, is both spatially and temporally varying. As a consequence, correction factors need to be found to compensate for these spatial and temporal variations to allow a valid comparison of $[O]_{Plasma}$ and $[O]_{Photolysis}$ and their corresponding TALIF signals for calibration purposes.

Various models have been developed that allow TALIF and photolysis to be simulated [20, 21, 26, 27]. The complexity of the model is mainly determined by the laser intensity range the model is applied over. For high laser intensities TALISE and REMPI have to be included in the model. Rabi flopping and the AC Stark shift are other high laser intensity effects that may have to be considered for very high intensities. As the laser intensity increases these effects along with ground state depletion all serve to make the laser power dependence of the TALIF signal deviate from a quadratic dependence and so are needed in the model.

In this work we investigate changes in atomic oxygen density in an air atmospheric plasma jet as the RF power coupled into the plasma increases. TALIF is used to measure the atomic oxygen density at each experimental condition. The TALIF system is calibrated using a new technique that allows in-situ calibration based on molecular oxygen photolysis. To implement the method a model is developed to determine correction factors R_z and R_t to account for spatial and temporal variation in the atomic oxygen density generated by photolysis allowing uniform invariant atomic oxygen densities such as those generated in plasma to be determined using the system. The model includes

TALISE, REMPI and ground state depletion effects so that the correction factors obtained will be accurate even for high laser intensity situations where the TALIF signals deviate from a quadratic laser power dependence. Using the values obtained for R_z and R_t from the model, [O] is determined in a 100 % dry air flow in the APPJ plasma plume near the nozzle exit at various RF powers. The calibration technique, rate equation model and [O] results obtained in the APPJ are presented and discussed in this paper.

2. Experimental setup

The plasma jet used in this work which has been described previously is shown in figure 1 [28]. The jet is an atmospheric pressure cross field jet (APCFJ) where gas flow is perpendicular to the electric field, and the plasma is expelled from the plasma production region via a nozzle. The jet is constructed from an 11 cm long Polyether Ether Ketone (PEEK) cylinder with an inner diameter of 16 mm and an outer diameter of 20 mm. A stainless steel pin of diameter 4 mm which terminates in a hemispherical tip of length 8 mm and tip diameter of 2 mm is located inside the cylinder. This pin acts as the powered electrode and is fixed at a separation of 3 mm from the outer grounded electrode. The power supply used on the system is capable of providing voltages of up to 20kV.

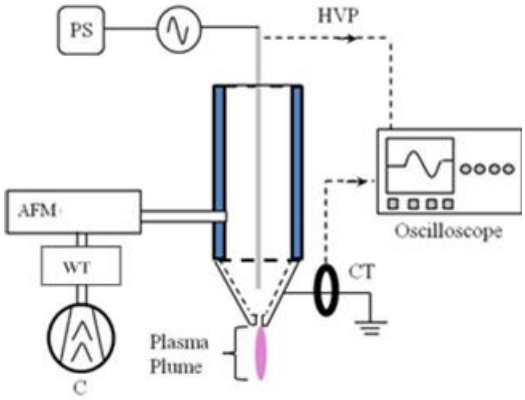

Figure 1: Plasma jet schematic diagram (Gogna [28]). PS-High voltage power supply, C - Air compressor, WT –water & oil vapour trap, AFM - Air flow monitor, CT - Current transformer, HVP - High voltage probe, SC - System controller.

Air is flowed into the system using a Clarke Wiz air compressor which is capable of producing an air displacement of 1.58 cfm and maximum pressure of 40 psi. A water vapour filter is included in the air line to prevent oil and water vapour from passing through the plasma jet. A SMC pneumatics PFM725S-C6-B digital flow switch is placed between the pump and plasma jet allowing the gas flow rate into the jet to be varied between 0.5 slpm and 25 slpm. In this work air was used as the gas source and [O] at the exit of the jet monitored using TALIF for various RF input powers.

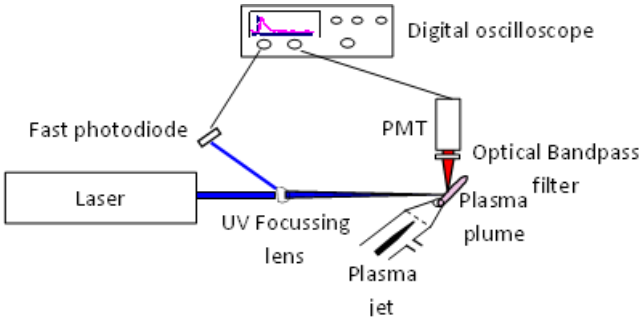

Figure 2: Schematic of the TALIF arrangement used in this work. The laser beam is focused in the plasma jet plume at 5mm from the exit orifice. The resulting fluorescence passes through an optical bandpass filter and is detected by a photomultiplier tube (PMT). A back reflection from the focusing lens is used to trigger the scope where both the TALIF and laser signals are recorded.

A schematic of the TALIF experimental arrangement is shown in figure 2. An Innolas Spitlight 600 Nd:YAG laser system which has a bandwidth of < 0.03 cm^{-1} operating at a frequency of 10 Hz was used to pump a Radiant Dyes Narrowscan dye laser. The second harmonic of the Nd:YAG laser which produces pulses of ~ 8 ns duration at 532 nm was used to pump a dye mixture of DCM/Pyridine 1 in methanol producing a useful lasing wavelength range of 640 nm - 705 nm. The output from the dye laser passes through a set of frequency doubling and tripling crystals before finally passing through a Pellin Broca prism system to separate out the UV radiation at 226 nm from the dye fundamental and doubled wavelengths. The laser output was focused into the plasma plume at a distance of 4 mm from the plasma jet exit using a UV grade fused silica plano-convex lens with a focal length of 438 mm at 225.6 nm. A back reflection from the focussing lens was steered onto a Thorlabs Det210 fast photodiode and used to trigger the oscilloscope. The laser interacts with atomic oxygen in the plasma via two-photon absorption resulting in fluorescence at 844 nm which was recorded at 90^o to the laser propagation direction using a Hamamatsu R636-10 photomultiplier tube. A LOT-Oriel optical bandpass filter centred at 844 nm with a 0.8 nm bandwidth was placed at the entrance to the photomultiplier tube (PMT) to attenuate all light except at the fluorescent wavelength.

Applying photolysis for TALIF calibration, the atomic oxygen density [O] can be found using the expression:

$$[O] = \chi \frac{S_O}{R_z R_t S_{Cal}} [O]_{Cal} \qquad (1)$$

where S_O and S_{Cal} are the atomic oxygen TALIF signals integrated with respect to time, fluorescent wavelength, excitation wavelength and normalised to the square of the laser pulse energy. S_O refers to the TALIF signal produced by atomic oxygen in the plasma, while S_{Cal} refers to the TALIF signal produced during the photolysis calibration. $[O]_{Cal}$ is the total atomic oxygen density generated at the focal point by laser photolysis. R_z and R_t are correction factors for the spatial and temporal variation in the photolysis atomic oxygen density. The constant χ is given by:

$$\chi = \frac{T_{Cal}}{T_O} \frac{\eta_{Cal}}{\eta_O} \frac{\sigma_{Cal}}{\sigma_O} \frac{{a_{ij}}^{Cal}}{{a_{ij}}^{O}} \left(\frac{\lambda_{Cal}}{\lambda_O}\right)^2 \qquad (2)$$

where T is the transmission of the optical components of the system, η is the quantum efficiency of the detector at the fluorescence wavelength, a_{ij} is the effective branching ratio for the transition and σ is the two-photon absorption cross section. Atomic oxygen is used for both calibration and measurement, so the constant χ can be greatly simplified as most of the constants in the ratio are identical and cancel out. The branching ratio a_{ij} however needs special attention as the oxygen atoms produced by photolysis are "hot" and so have a significantly larger velocity than oxygen atoms produced in a plasma. The hot oxygen atoms will experience enhanced quenching due to their larger velocity so the branching ratio a_{ij} will not be the same in both cases and do not directly cancel. The constant χ can thus be rewritten as $\chi = a_{ij}^{Cal}/a_{ij}^{O}$.

Signals from the PMT and photodiode were recorded using a Tektronix DPO 3034 300 MHz digital oscilloscope. All data was taken using a LabVIEW programme interfaced to the dye laser and oscilloscope. The laser wavelength was scanned across the atomic oxygen transition in all cases and the resulting TALIF signal integrated with respect to time, wavelength and normalized to the square of the laser pulse energy. The programme set the laser wavelength and recorded the resulting TALIF signal and laser back reflection signal for each laser pulse. The TALIF and laser signals were integrated, the TALIF signal normalized to the square of the laser signal, and the resulting normalized TALIF signals averaged. This process was repeated for each wavelength over a spectral scan range of 225.6475 nm - 225.6670 nm. The resulting data was used to generate spectral profiles which were then integrated with respect to wavelength to give the quantity S_i for each experimental condition.

The laser output power was measured using a FieldMaxII TO power meter with a PM3 power sensor head. The laser was fired at 10 Hz allowing the energy per laser pulse, E_{pulse}, to be found. The focal spot area A was determined by firing the laser onto black photography paper placed at the focal plane. The resulting spot size was measured using a microscope thus allowing the laser intensity at the focal

point to be determined. The laser pulse traces recorded on the scope were averaged and fit to a Gaussian with a Full Width Half Maximum (FWHM) value τ_{FWHM} of 4.46 ns (see figure 4 (a)) allowing the laser intensity $I_0(t)$ to be found as a function of time which is required in our rate equation model to determine R_t. $I_0(t)$ is given by the expression:

$$I_0(t) = \frac{E_{pulse}}{A\tau_{FWHM}} . \sqrt{\frac{4\ln(2)}{\pi}} . exp\left[\frac{-4\ln(2)}{{\tau_{FWHM}}^2}(t - t_0)^2\right] \qquad (3)$$

In these experiments the dye laser pulses produced a power output of 1.2 mW at 225.56 nm, giving a laser pulse energy of 0.12 mJ per pulse. The laser pulse energy was found to fluctuate by ~ 13 % during experiment. The laser wavelength λ_{Laser} was set at ~ 225.65 nm giving a photon energy of ~ 5.5 eV which is sufficiently large to cause photo-dissociation of molecular oxygen ($E_{diss}(O_2)$ = 5.17 eV). The laser beam was focused down to a focal spot area of 6.03×10^{-9} m^2 using a fused silica lens giving a total beam intensity of 2×10^5 W/m^2 at the focal point. As the laser is fired at 10 Hz the "intensity per pulse" has a value of 2×10^4 W/m^2. All future references to laser intensity in this work will relate to the intensity per pulse. The atmospheric pressure, temperature and relative humidity in the laboratory were recorded on the day (atm. Pressure = 1.013×10^5 Pa, temperature = 291 K, humidity 0.45) and the molecular oxygen density in the air calculated for calibration purposes. The plasma temperature was measured using a K-type thermocouple for each plasma setting investigated in this work

3. Theory and Discussion.

The plasma jet used in this work has been previously investigated by Gogna et al [28]. They used mass spectrometry to investigate the chemical composition of an air APPJ produced by the system. They found that ozone (O_3) and nitric oxide (NO) were the dominant species present in the jet. The ratio of ozone density [O_3] to nitric oxide density [NO] was found to be a strong function of distance from the nozzle with [NO] dominating near the nozzle, and [O_3] becoming more dominant with distance from the nozzle while [NO] decreased. They also found that [O_3] was strongly affected by the power coupled into the plasma with [O_3] dropping with increasing power. The lower limit of detectability of the mass spectrometry system was 10 ppm, so other species could be present at densities below the detection threshold of the mass spectrometer system used. To further characterize the air plasma in this system an investigation into atomic oxygen density [O] was carried out near the nozzle where ozone density is minimal using TALIF experiments. [O] was measured as a function of RF power into the plasma.

TALIF experiments to determine atomic oxygen density involve focussing a tuneable laser with a central wavelength of 225.65 nm into the plasma at the point of interest. The high intensity of photons at the focal point enables two-photon absorption by oxygen atoms in the focal region which then give off fluorescence at 844 nm (see figure 3).

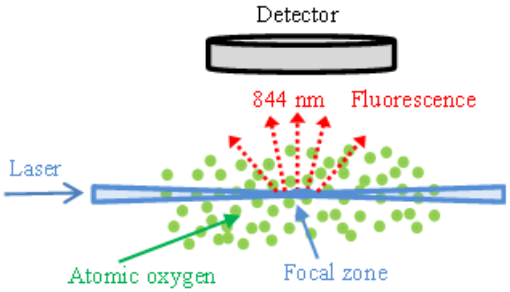

Figure 3: The 225.65 nm laser beam is focussed into the plasma where it interacts with the atomic oxygen in the plasma. The detector records the resulting 844 nm fluorescence at 90° to the direction of propagation of the laser.

If the laser intensity is kept sufficiently low so that saturation effects are negligible, the total number of fluorescent photons emitted per unit volume η_f is directly related to the atomic oxygen density in the plasma in the focal zone by the expression:

$$n_f = \frac{A_{ij}}{A_i+Q_i}\frac{\sigma^{(2)}}{(hf)^2}G^{(2)}g(\omega)[O]\int_0^t {I_0}^2(t)dt \quad (4)$$

where A_{ij} is the transition rate of the upper level for the fluorescence wavelength, A_i is the total transition rate from the upper level i, Q_i is the quenching coefficient of the upper level, f is the laser frequency, $\sigma^{(2)}$ is the two-photon absorption cross section, $G^{(2)}$ is the photon statistic factor, $g(\omega)$ is the normalized line profile, *[O]* is the atomic oxygen density, and $I_0(t)$ is the laser intensity. The laser profile function $g(\omega)$ was determined from experimental TALIF spectral profiles plotted as a function of angular frequency ω. The resulting profile was integrated to find the area under the curve, and the spectral profile was then divided across by the area giving the normalized line profile $g(\omega)$. The value at the line centre $g(\omega_0)$ was determined to be 4.5×10^{-12} s. Using the laser intensity function $I_0(t)$ given in equation (3) in conjunction with values for the constants A_{ij}, A_i, Q_i, $G^{(2)}$ and $\sigma^{(2)}$ taken from references [11] and [29], η_f can be calculated for a steady state uniform oxygen density [O].

To determine absolute atomic oxygen values in plasma, the TALIF system must be calibrated. This is often done using a well-established xenon gas TALIF scheme that has similar excitation and fluorescent wavelengths to the atomic oxygen TALIF scheme [11, 18]. Successful application requires operating the laser at low intensities which can present problems at atmospheric pressures as strong quenching effects diminish the TALIF signal. A further consideration is that xenon is expensive, so flowing it through atmospheric pressure systems for calibration purposes is costly. Photolysis of molecular oxygen was chosen for TALIF calibration in this work. Adopting this approach means atomic oxygen is the target species probed by TALIF during calibration and measurement which has several advantages. Both the calibration and measurement procedures are performed with identical temporal, spatial and spectral intensity distribution in the laser beam as the laser wavelengths used to probe [O] during each procedure will be the same. As a result, there is no issue with variation in laser performance when operated at different wavelengths. Another advantage is that the fluorescence wavelength produced during calibration and experiment will be identical so there is no error associated with detector sensitivity at different wavelengths. Also, the optical bandpass filter used to attenuate background light from reaching the detector will require the same central wavelength in both cases, meaning that the bandwidth of the filter need only be wide enough to accommodate the linewidth (FWHM < 1nm) of the resulting atomic oxygen fluorescent line. The narrow bandwidth reduces the amount of background light reaching the detector improving signal to noise ratio. A further advantage is that TALIF experiments can be carried out at higher laser powers, as any saturation effects (e.g. REMPI) that occur will be identical during the calibration and measurement procedures as atomic oxygen is used in both cases. This ensures that the laser power dependence of the TALIF signals remain the same, even at higher powers. Operating the laser at higher intensities produces stronger TALIF signals allowing us to overcome the problem of weak TALIF signals that have been encountered with ns laser pulses when using xenon calibration in atmospheric pressure plasma systems.

When photons with energy exceeding the dissociation energy of molecular oxygen (5.17 eV) are absorbed by O_2 molecules, dissociation can occur resulting in two oxygen atoms. The dissociation yield for O_2 is 100 % so the atomic oxygen density produced by a laser pulse during photolysis is given by the expression [25]:

$$[O] = 2[O_2](1 - \exp(-\sigma\phi)) \quad (5)$$

where σ is the photo-dissociation cross section at λ_{Laser}, and ϕ is the photon fluence given by the equation:

$$\phi = \int_0^t \frac{I_0(t)}{hf} = \frac{E_{pulse}}{hfA} \quad (6)$$

where E_{pulse} is the laser pulse energy, f is the laser frequency, h is Plancks constant, A is the area of the laser focal spot and $I_0(t)$ is the laser beam intensity. Single photon absorption in the Herzberg continuum of O_2 ($\sigma = 3 \times 10^{-24}$ cm^2 at 225.6 nm [30]) results in photo-dissociation of O_2 producing two ground state $O(^3P_2)$ atoms. For a laser intensity of 2×10^4 W/m^2 per pulse, laser photolysis yields an oxygen density $[O]_{Cal}$ of 7.12×10^{19} m^{-3} per pulse. The error on this value was estimated to be ~ 21 %, mainly due to laser energy fluctuations.
Using equation (4), the fluorescent photon density $\eta_{f\,Cal}$ due to a steady state uniform oxygen density with value $[O]_{Cal}$ can readily be found. However, the atomic oxygen density produced by photolysis, [O](t), is a function of time and increases over the course of the laser pulse before reaching its final value of 7.12×10^{19} m^{-3} . To take account of this, equation (4) is modified to find the fluorescent density $\eta_f(t)$ due to a time varying atomic oxygen density giving:

$$n_f(t) = \frac{A_{ij}}{A_i+Q_i}\frac{\sigma^{(2)}}{(hf)^2}G^{(2)}g(\omega)\int_0^t [O](t){I_0}^2(t)dt \qquad (7)$$

The time varying atomic oxygen density [O](t) was calculated using equations (5) and (6) and is shown in figure 4(b). Similarly, using equations (4) and (7), simulations were carried out to model TALIF fluorescent photon densities $\eta_f(t)$ and η_{fCal}. These results are shown in figure 4 (c). The fluorescent photon density $\eta_f(t)$ is clearly less than η_{fCal}, so a correction factor R_t needs to be found to allow the TALIF signals be related to each other. Comparing the fluorescence photon density produced per laser pulse from $[O]_{Cal}$ to the fluorescence photon density produced per laser pulse from [O](t) by a similar laser pulse allows the correction factor R_t to be determined.

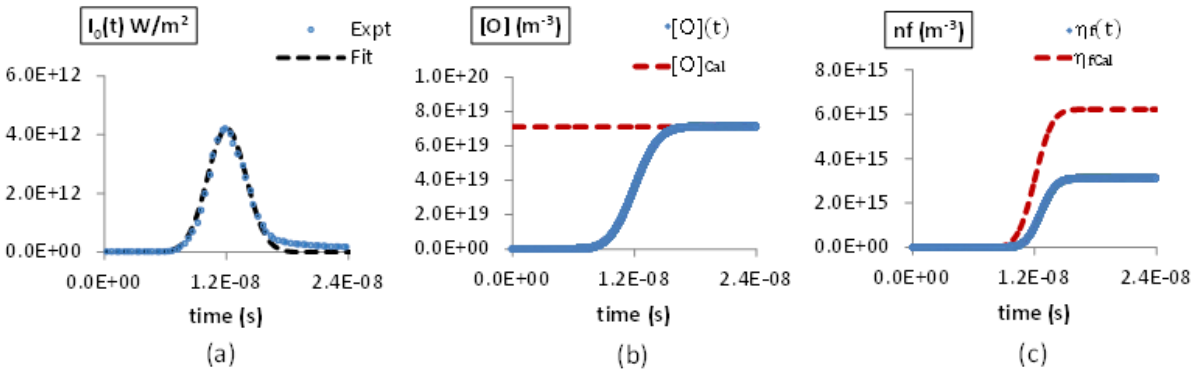

Figure 4: (a) Plot of the experimental laser intensity profile recorded, and the corresponding Gaussian fit $I_0(t)$. The delayed roll off in the experimental data is a result of the response function of the photodiode. (b) Simulation results for atomic oxygen density [O](t) and $[O]_{Cal}$ produced by photolysis (c) Simulation results for the fluorescent photon density $\eta_f(t)$ and η_{fCal} produced over the duration of the laser pulse.

Using equation (4) and (7) and taking the ratio of the photon densities (i.e. $n_{fcal}/n_f(t)$) for the fixed density population to the time varying O population over the entire laser pulse (i.e. $t = \infty$) gives:

$$R_t = \frac{n_{fCal}}{n_f(t)} = \frac{[O]_{Cal}\int_0^\infty {I_0}^2(t)dt}{\int_0^\infty [O](t){I_0}^2(t)dt} \qquad (8)$$

In this work we include high laser intensities that take the TALIF signal's laser power dependence outside the quadratic region, so saturation effects need to be included to get reliable R_t values for all laser intensities considered. Equations (4) and (7) only relate to unsaturated TALIF signals, so to determine the fluorescent photon density as a function of time, a model was developed which involved solving a set of coupled differential rate equations using Runge-Kutta 4 methods. The model included high intensity effects due to REMPI, TALISE and ground state depletion so that the

correction factor R_t can be determined for laser intensities that fall outside the quadratic region such as may be needed at atmospheric pressures. Details of the model are included in the appendix. The resulting R_t values obtained using the model are given for various laser pulse intensities and FWHM values in figure 5. Selecting the R_t value from figure 5 corresponding to the laser pulse intensity and FWHM used, the photolysis TALIF signal S_{Cal} to be corrected for the time varying nature of [O](t) allowing S_{Cal} to be related to TALIF signals S_O produced by plasma atomic oxygen densities $[O]_{Plasma}$.

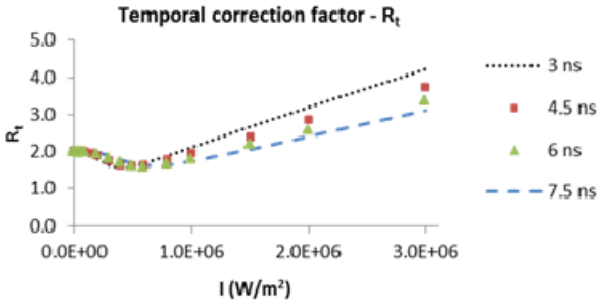

Figure 5: Temporal correction factor R_t calculated using the rate equation model for the laser intensities and FWHM values shown. The model includes REMPI, TALISE and ground state depletion.

The laser beam used in these experiments was focused into the plasma near the nozzle exit to measure [O] at that point. One consequence of lensing is that laser intensity varies with distance as the beam travels from the lens toward the focal point, so the atomic oxygen density produced during photolysis, [O](z), is non-uniform and varies with position across the focal zone (see figure 6).

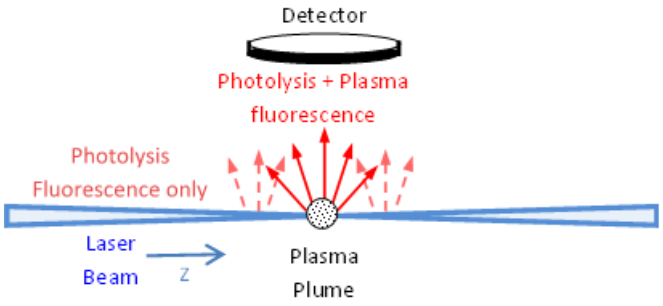

Figure 6: The laser beam (z-direction) is focused onto the plasma plume. The number of TALIF photons reaching the detector from outside the plasma plume (faded dashed arrows) will be identical for plasma-on and plasma-off. The number of TALIF photons coming from within the plume (solid arrows) will change depending on whether the plasma is on or off.

[O](z) has a value of $[O]_{Cal}$ (7.12×10^{19} m^{-3}) at the focal point and drops off with distance on either side of the focal point. As a result, a spatial correction factor R_z needs to be found to allow TALIF signals due to [O](z) be compared to the TALIF signal due to a uniform density of value $[O]_{Cal}$. The laser beam radius $w(z)$ for a focused Gaussian laser beam at a distance z from the beam waist w_0 is given by the expression:

$$w(z) = w_0\sqrt{1 + \left(\frac{z}{Z_R}\right)^2} \qquad (9)$$

where the Rayleigh distance Z_R is given by $\pi {w_0}^2/\lambda$, z is the distance from the beam waist. Applying this equation allows the laser beam intensity $I_0(z)$ to be found as a function of distance z across the detector zone. The atomic oxygen number density [O](z) can then be found using equation (5) and is shown along with $[O]_{Cal}$ in figure 7. The detector which has a 25 mm diameter was centred over the

focal point to detect fluorescent photons produced by the laser pulse. The fluorescence density η_f produced across the detector zone can be calculated using $I_0(z)$ in equation (4) for points along the optic axis. The TALIF photon density $\eta_f(z)_{Cal}$ produced over the detector zone by a uniform atomic oxygen density of value $[O]_{Cal}$ and the TALIF signal $\eta_f(z)$ from the spatially varying oxygen population [O](z) are both shown in figure 7. Taking the ratio $\eta_f(z)_{Cal}/\eta_f(z)$ allows a spatial correction factor R_z to be determined. An R_z value of 1.06 was found for the experimental set-up used in this work so differences in the TALIF signal due spatial variation in the photolysis atomic oxygen population are small. This analysis assumes a perfectly focussed Gaussian beam. However the measured focal spot had a diameter of ~ 80 μm which is somewhat bigger than expected for a perfect Gaussian beam (~ 70 μm) leading to an error of ~ 7 % in the value of R_z obtained using the model. The laser cuts the plasma plume radially and any TALIF signal due to $[O]_{Plasma}$ are confined to the plasma region. Any TALIF signals generated outside the plasma zone are due to photolysis and are identical for plasma-on and plasma-off, so they are removed during background signal subtraction.

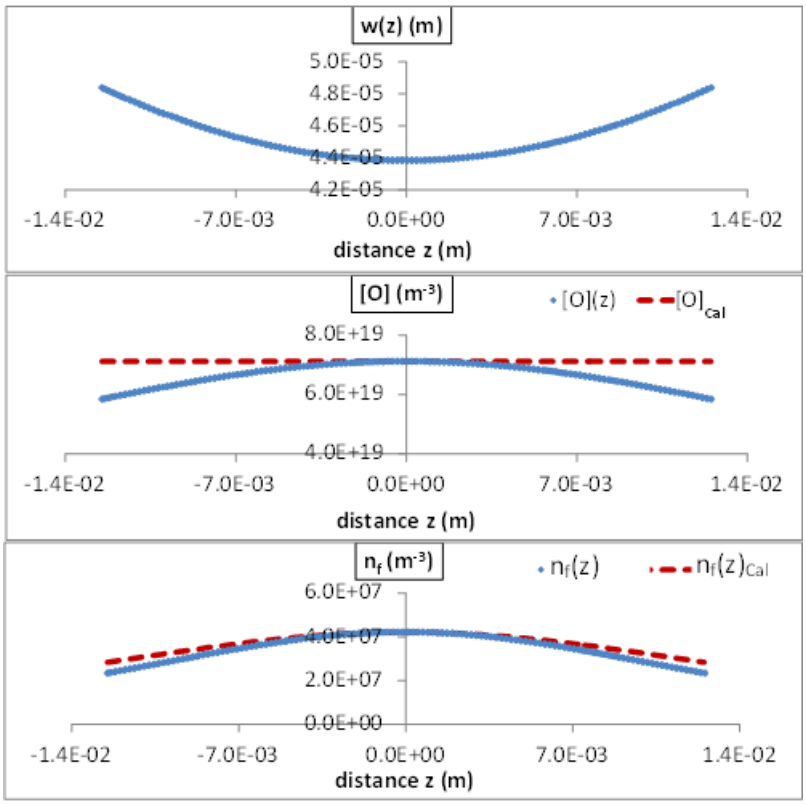

Figure 7: Simulation results for the laser beam radius w(z), atomic oxygen density, and fluorescent photon density as a function of distance around the focal point over a 25 mm distance. R_z is found using the ratio $n_f(z)_{Cal}/n_f(z)$ and has a value of 1.06.

The branching ratio introduced in equation (1) is given by the expression:

$$a_{ij} = \frac{A_{ij}}{(A_i+Q_i)} \tag{10}$$

where the quenching factor Q_i is given by the expression:

$$Q_i = \sum_q k_q^i n_q \tag{11}$$

where $n_q$is the number density of quenching species q, and $k_q^i = \sigma_q^i\langle v\rangle$ is the corresponding quenching coefficient. The quenching coefficient depends on the collisional cross section σ_q^i and the

mean collisional velocity $\langle v \rangle$ of the quenching partners. The laser photons at 225.6 nm have energy of 5.5 eV while the dissociation energy of molecular oxygen is 5.17 eV so the excess energy of 0.33 eV is divided between the two oxygen atoms produced during photolysis due to the Frank-Condon effect. As a result these atomic oxygen atoms have velocities $\langle v \rangle_{hot}$ of 1411 m/s and are substantially faster than oxygen atoms produced in the plasma which have mean velocities $\langle v \rangle$ of ~ 600 m/s assuming a gas temperature of 300 K. The fast O atoms will experience larger quenching resulting in a smaller branching ratio than the cooler plasma generated O atoms. The main quenchers in air are N_2, O_2 and Ar as these constitute 78 %, 20.9 % and 9 % of the atmosphere respectively so the quenching factor for atomic oxygen in air can be written as:

$$Q_i = [(0.78)\, k^i_{N_2} + (0.209)\, k^i_{O_2} + (0.009)\, k^i_{Ar}] \times \frac{Patm}{kT} \qquad (12)$$

The quenching coefficients and the resulting branching ratios for the "hot" and "cool" oxygen atoms are listed in table 1. The constant $\chi = a^{cal}_{ij}/a^{O}_{ij}$ is found to have a value of 0.5564 using the branching ratios calculated. To estimate the uncertainty in the value for the branching ratio, error values for the quenching coefficients and radiative lifetime were taken from references [7] and [11], and yielded an uncertainty of ~ 15 % for χ due to the error in the branching ratio values.

O	N_2 ($cm^{-3}s^{-1}$)	O_2 ($cm^{-3}s^{-1}$)	Ar ($cm^{-3}s^{-1}$)	a_{ij}
k^i_q (300 K)	5.9×10^{-10}	9.4×10^{-10}	1.4×10^{-11}	1.753×10^{-3}
k^i_q (O Hot)	10.5×10^{-10}	17.2×10^{-10}	0.27×10^{-10}	9.753×10^{-4}

Table 1: The quenching coefficients for the main quenchers in air are given for a gas temperature of 300 K [7, 11]. The quenching coefficients corrected for hot O atoms produced during photolysis are also included along with the resulting branching ratio for each case. The branching ratio is almost halved due to the enhanced quenching experienced by the hot O atoms.

A further consideration is that both the lower and upper TALIF energy levels of oxygen are not singlet states and are in fact triplet states. The ground state of oxygen $O(2p^4\ ^3P_{2,1,0})$ has a well separated triplet structure. Only one of these (J = 2) is probed during the TALIF experiment so only a fraction of the total oxygen population is measured during the TALIF experiment. To get the total ground state population of oxygen atoms a Boltzmann thermal distribution is assumed which is given by:

$$\frac{n_J}{\sum_J n_J} = \frac{(2J+1)\exp(-E_J/k_B T_g)}{\sum_J (2J+1)\exp(-E_J/k_B T_g)} \qquad (13)$$

where k_B is the Boltzmann constant, E_J is the energy level of each of the ground level triplet states and T_g is the gas temperature. This allows the fraction of the oxygen measured during TALIF to be determined enabling the total oxygen density to be found. For a gas temperature of 291 K the probed level makes up ~ 74.7 % of the total ground state atomic oxygen population.

Fly-out, where some of the oxygen atoms created during photolysis may exit the focal zone during the laser pulse before two-photon absorption occurs may also be an issue [25]. The laser pulse has an 8 ns duration, so the hot O atoms can travel up to 11.3 μm meaning that ~ 45 % of the oxygen atoms could leave the focal zone during the laser pulse. However, at atmospheric pressure the mean free path λ is small (λ ~ 66 nm) so the root mean square distance X_{RMS} travelled is substantially reduced. X_{RMS} is given by the expression $X_{RMS} = \sqrt{4Dt}$ where t is the travel time and $D = 1/3\lambda\langle v \rangle_{hot}$ is the diffusion coefficient so X_{RMS} is 9.95×10^{-7} m. As a result 99.5 % of the oxygen will remain in the focal zone over the laser pulse and contribute to the TALIF signal generated. This assumes the laser beam has a perfect flat-top spatial profile so the atomic oxygen density generated during photolysis is uniformly distributed across the focal region. However, laser beams are often more intense near the beam centre with the intensity falling off toward the beam edge. As a result the atomic oxygen density generated by photolysis is not uniformly distributed in the focal zone with the density being higher near the

centre and diminishing toward the edge where fly-out occurs. As a result, the atomic oxygen loss during the laser pulse will be less than that estimated in the analysis using a perfect flat-top profile, so our approach gives an upper estimate of the fly-out loss.
Taking the various factors discussed into account, equation (1) can be written as:

$$[O] = \frac{(0.5564)}{(0.995)(0.747)} \frac{S_O}{R_z R_t S_{Cal}} [O]_{Cal} \qquad (14)$$

This calibration approach can also be used in low pressure systems if atmospheric air is introduced by venting the system to air, allowing a photolysis TALIF signal to be measured. The system can then be pumped down and atomic oxygen TALIF measurements made using the calibrated TALIF system.

4. Results.

Using the intensity per pulse value of 2×10^4 W/m^2 measured, the calibration oxygen density $[O]_{Cal}$ was calculated to be 7.12×10^{19} m^{-3}. The laser pulse has a FWHM of 4.46 ns so referring to figure 5 the correction factor R_t was found to have a value of 2 for this laser pulse intensity and width. While the laser pulse energy was found to fluctuate by ~ 13 % over the course of the experiment, the model shows that the R_t value remains at 2.000 when the laser intensity in the model is varied by this amount, so the laser fluctuations have no noticeable effect on R_t to three decimal places at the laser intensity level used. The spatial correction factor R_z was found to be 1.06 for the laser focussing conditions used in this work.

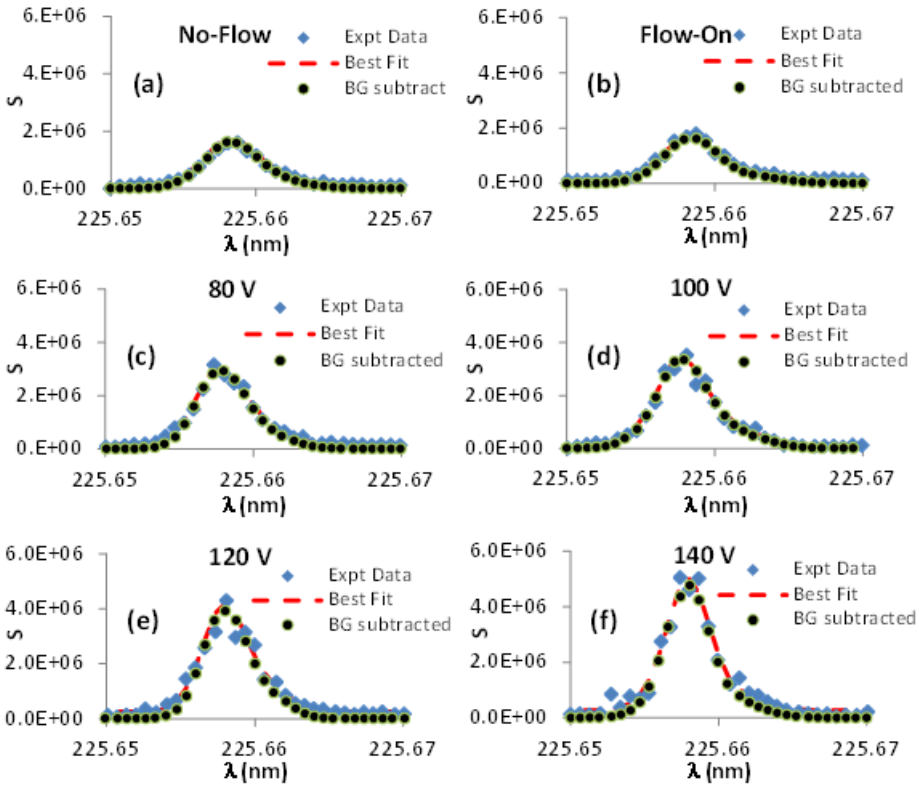

Figure 8: TALIF signals recorded along with line profile fits. Background subtraction was used to remove any DC bias level. (a) in air with no gas flow or plasma. (b) air flow on and no plasma. (c) – (f) plasma-on for the conditions as labelled above.

The air flow was turned on, fixed at 8 slpm, and a TALIF scan performed for calibration purposes to find S_{Cal}. This also served as the background TALIF signal S_{BG} which was subtracted from all subsequent TALIF measurements made with the plasma on to extract the TALIF signal due to atomic oxygen originating in the plasma, S_o. Once these initial measurements were made, the plasma was turned on and the RF power coupled at 12 kHz into the atmospheric jet varied between 5W and 20 W

by altering the voltage on the plasma RF power supply while keeping the air flow at 8 slpm. A TALIF scan was performed at each of the power settings. The resulting experimental TALIF traces are shown in figure 8. The recorded TALIF line is made up of contribution from each state of the of the $O(2p^4\ ^3P_{1,2,\ 0})$ excited level. A superposition of Gaussian profiles for each of the excited states was fit to the recorded TALIF profile using excel solver. The resulting best fit profile was integrated to find the TALIF signal S_i and the TALIF signal $S_o = S_i - S_{BG}$ was calculated for each of the RF power setting examined in this work. The error in the resulting S values was calculated to be ~ 20 %.
The plasma plume temperature was recorded at each experimental setting with a K-type thermocouple. With no plasma, the air flow temperature was measured to be 21 ^oC. With plasma on, the temperature was found to increase from 52 ^oC at 80 V up to 71 ^oC at 140 V. The branching ratios were calculated for each plasma condition to account for the changes in temperature, and the resulting [O] values calculated using equation (14). The results are shown in figure 9 below. The overall error in atomic oxygen density was estimated to be ~ 42 % in these experiments. The TALIF results show that increasing the RF power over this range increases the atomic oxygen density in the plasma plume near the nozzle exit by a factor of ~ 3 on our system.

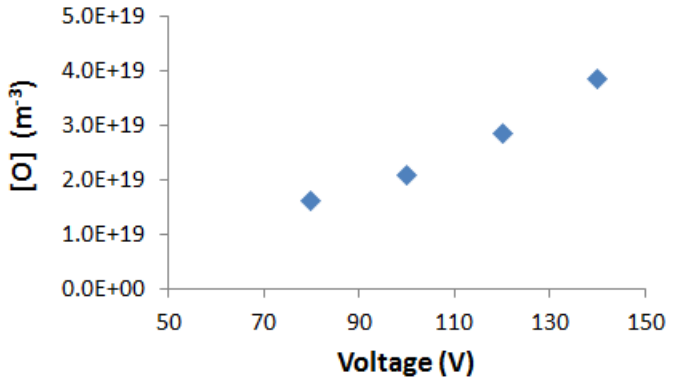

Figure 9: TALIF results for atomic oxygen density [O] as a function of the RF power supply voltage. Note that the voltages in the figure represent the voltage on the primary of a transformer and do not represent the actual voltages driving the plasma. As the RF power supply voltage increases the atomic oxygen density increases by a factor of ~ 3.

Previous work [22, 24] has shown that photolytic interference from oxygen containing molecules can lead to artificially high [O] values during TALIF experiments. For atmospheric air, O_2, CO_2 and water vapour are the main possible problem molecules. A TALIF signal resulting from photolysis of O_2 is expected and is in fact required to allow calibration of the system using the technique proposed in this paper. However, TALIF signals generated as a result of photolysis of H_2O vapour and CO_2 are considered nuisance signals that will affect the accuracy of the results. Water vapour content in the air flow from the jet is removed by a filter incorporated into the gas line to remove both water and oil vapour from the air flow. CO_2 will not present a problem as the laser photon energy at 226 nm is insufficient to photo-dissociate CO_2 ($E_{diss.}$ = 5.52 eV). With the plasma turned on, the chemical composition of the plasma jet flow becomes far more complex and new species formed in the plasma may result in extra atomic oxygen production by photolysis. Previous work by Gogna et al. [28] has shown that the main species present in a dry air plasma jet produced using our system are NO and O_3. The laser photons at 226 nm do not have sufficient energy to photo-dissociate NO molecules ($E_{diss.}$ = 6.55 eV) so photolysis of O_3 is the main possible source of error. Oxygen atoms produced during photolysis of O_3 by photons at 226 nm have large energies (~ 2.92 eV) due to the small dissociation energy of O_3 resulting in velocities of ~ 5940 m/s for the hot O atoms produced. As a result, these 'hot' atoms experience very strong collisional quenching. Comparing the branching ratio for O atoms at 300 K to that of hot O produced during O_3 photolysis, the hot O fluorescence will be 0.132 that of O atoms at 300 K so any fluorescence signal produced by the hot O atoms will be strongly reduced. Furthermore, the hot O population produced during the laser pulse via O_3 photolysis will be a function of time over the duration of the pulse, so the resulting TALIF signal will be ~ 0.5 that produced by an equivalent steady state O population, in the same manner as the calibration TALIF signal produced by

O_2 photolysis. Finally, any fluorescence emitted by the hot O will be strongly Doppler broadened reducing the strength of the TALIF signal at 226 nm and extending the wings of the absorption profile. However, an inspection of the TALIF profiles in figure 8 show no evidence of hot O atoms in the wings of the two-photon excitation line profile. The lack an O_3 signature in the TALIF signal is consistent with previous work which has shown [O_3] to be low near the plasma jet nozzle, and increase with distance from the nozzle [13, 28]. Other work has shown that atomic O content is strongest near the nozzle, and decreases with distance from the nozzle [7, 11, 13, 15]. Our measurements at a distance of 4 mm from the nozzle show a measurable [O] presence near the nozzle with little evidence of ozone present which is consistent with the previous work done.

Previous oxygen density measurements on plasma jets have shown [O] densities ranging from ~10^{19} – 10^{22} depending on the jet type and gas mixture used. Jiang and Carter recorded [O] values of ~10^{19} m^{-3} in ns pulsed jet using a He/O_2 gas flow containing 1% O_2 [12]. Ziang however measured values of ~ 10^{22} m^{-3} in a power modulated RF APPJs using Ar/air and Ar/O_2 admixtures containing 2% O_2 and 2% air respectively, a result that agrees well with that of Van-Gessell using a He/air mix with 1 – 6 % air [7, 13, 15]. Schmidt measured [O] values of ~ 10^{21} m^{-3} in a ns pulsed APPJ using gas flows of He/O_2 containing 2 – 4 % O_2 [22]. While the [O] result measured in this work are at the lower end of the scale, it has been found previously that [O] decreases in APPJs as the percentage of [O_2] in the gas flow increases, so in an 100 % air flow containing ~ 20 % O_2, the atomic oxygen density [O] is expected to be somewhat smaller than that measured in plasma jets with 1 – 5 % O_2 or air in the gas flow [6, 7, 22].

The atomic oxygen density produced in the plasma jet increases with RF power, a trend that agrees with previous measurements of [O] in other plasma jet systems [22, 31]. This is expected as previous work on plasma jets has shown that the electron density increases with RF power [32, 33]. The production rate of atomic oxygen in a plasma is given by $Rn_e[O_2]$ where R is the rate constant, n_e is the electron density and [O_2] is the molecular oxygen density. As n_e increases [O] in the jet should also increase.

Conclusion

Atomic oxygen number density has been measured in a 100 % dry air flow APPJ using TALIF. A new calibration technique using photolysis of O_2 was applied to determine the absolute atomic oxygen number density in the plasma under various operating conditions. Use of this calibration method involved analysis of both the temporal development, and spatial non-uniformity of the atomic oxygen produced during photolysis. A rate equation model was used to find the temporal correction factor R_t while the laser beam focussing in the focal zone was examined to find a spatial correction factor R_z. The correction factors allow valid comparison of photolysis atomic oxygen densities to those produced in plasma, which are essentially temporally invariant and spatially uniform. A graph of R_t values was found that can be used once the laser intensity per pulse and the FWHM are known allowing easy photolysis calibration of atomic oxygen TALIF experiments. No benchmarking experiments were performed to validate the [O] results obtained. The atomic oxygen density in the plasma jet was found to increase with RF power.

Acknowledgements: This material is based upon work supported by Enterprise Ireland under Grant no. IP/2013/0267. I would like to thank Dr Sean Kelly for his helpful discussions on the previous work done on the jet system. I would also like to thank Mr Conor Murphy for his technical assistance with these experiments.

Appendix

A rate equation model was used to determine a temporal correction factor R_t to allow photolysis be used to calibrate a TALIF system. The correction factor gives the ratio of the TALIF signal produced by a stable uniform oxygen density with value $[O]_{Cal}$, the atomic oxygen density produced by photolysis at the focal point as given by equation (5), to the TALIF signal from the time varying oxygen density [O](t) produced by photolysis.. The model consists of a set of coupled rate equations that allow for (i) two-photon excitation by 225.6 nm radiation (ii) Spontaneous emission at 844 nm (iii) collisional quenching due to atmospheric O_2, N_2 and Ar (iv) REMPI due to three-photon absorption of 225.6 nm radiation (v) TALISE at 844 nm due to population inversion of the energy

levels 3 and 2 during the laser pulse and (vi) ground state depletion in atomic oxygen (see figure 1A). As saturation effects are included in the model the R_t values obtained are expected to be reliable even at higher intensities. A coupled rate equation approach to this problem can be used provided the Maxwell-Bloch equations can be uncoupled from the laser radiation field which is required for a complete description of the problem. One way to ensure the rate equation approach is valid is if there are many collisions during the laser pulse so that the coherence of the laser field is decoupled from the atoms [27, 34, 35]. At atmospheric pressure a large collisional frequency (~ 10^{10} s^{-1}) is guaranteed justifying the use of coupled rate equations for the model.

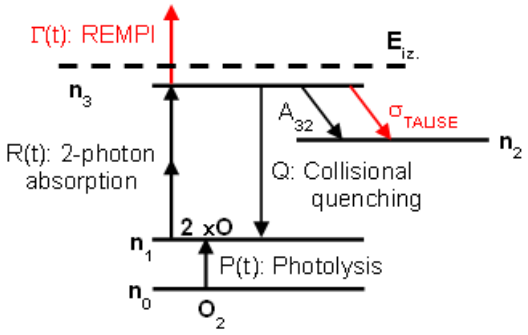

Figure 1A: The various atomic processes included in the model are shown. Two-photon absorption, spontaneous emission, REMPI, TALISE, photolysis of O_2 and collisional quenching are all included.

Rate equations (1A) – (6A) give the density for O_2, $O(2p^4)$, $O(3s^1)$, $O(3p^1)$, the TALISE photon density η_{ASE} and O^+ as a function of time over the laser pulse duration:

$$\frac{dn_0}{dt} = -n_0(t)\frac{\sigma}{h\nu}I(t) \tag{1A}$$

$$\frac{dn_1}{dt} = -R(t)[n_1(t) - n_3(t)] + Qn_3(t) + A_{21}n_2(t) + \boldsymbol{P(t)n_0(0)} \tag{2A}$$

$$\frac{dn_2}{dt} = A_{32}n_3(t) - A_{21}n_2(t) + \mathrm{G}\sigma_{ASE}cn_4(t)[n_3(t) - n_2(t)] \tag{3A}$$

$$\frac{dn_3}{dt} = R(t)[n_1(t) - n_3(t)] - \big(Q + A_{32} + \Gamma(t)\big)n_3(t) - \mathrm{G}\sigma_{ASE}cn_4(t)[n_3(t) - n_2(t)] \tag{4A}$$

$$\frac{dn_4}{dt} = \mathrm{G}\sigma_{ASE}cn_4(t)[n_3(t) - n_2(t)] - \frac{n_4(t)}{t_z} + \frac{\Omega}{4\pi}A_{32}n_3(t) \tag{5A}$$

$$\frac{dn_5}{dt} = -\Gamma(t)n_3(t) \tag{6A}$$

where *G* refers to a gain factor which takes into account amplification of the TALISE signal as it passes through the plasma region while the laser pulse is interacting with the plasma (i.e. while a population inversion exists between level 3 and level 2), *c* is the speed of light, t_z is the time a photon takes to leave the plasma plume, $\Omega/4\pi$ is the fraction of isotropic spontaneous emission that travels in the same direction as the laser beam (i.e. in the direction the TALISE radiation travels). The photolysis dissociation rate P(t), two-photon excitation rate R(t) and three-photon REMPI ionization rate Γ(t) and gain factor G are respectively given by:

$$P(t) = 2.\frac{\sigma}{hf}\exp\left(\frac{-\sigma E(t)}{hfA}\right).I_0(t) \tag{7A}$$

$$R(t) = \frac{G^{(2)}\sigma^{(2)}g(\omega)}{(hf)^2}{I_0}^2(t) \tag{8A}$$

$$\Gamma(t) = \frac{\sigma_{iz}}{hf} I_0(t) \quad (9A)$$

$$G = \exp[(n_3(t) - n_2(t))\sigma_{ASE} z] \quad (10A)$$

where σ_{iz} refers to the REMPI cross section ($\sigma_{iz} = 5.3 \times 10^{-23}$ m^2) and σ_{ASE} refers to the TALISE cross section ($\sigma_{ASE} = 2.01 \times 10^{-16}$ m^2) and z refers to the effective length of the active medium [27]. The fluorescent photon density for any run of the model can then be found using:

$$\eta_f = A_{32} \int_0^\infty n_3(t) dt \quad (11A)$$

The rate equations were solved using a 4th order Runge-Kutta approach solved over a 24 ns time interval using a time step of 5×10^{-4} ns with the laser pulse centred at 12 ns. To find η_{fCal}, equations (2A) – (6A) were solved with the dissociation term $\boldsymbol{P(t)n_0(0)}$ excluded from equation (2A) and the initial n_1 value (i.e. $n_1(0)$) set equal to the $[O]_{Cal}$ value found using equation (5).
To find $\eta_f(t)$ equations (1A) – (6A) were solved with the dissociation term included and $n_1(0)$ set equal to zero. The resulting $n_3(t)$ densities were then multiplied by A_{32} and integrated to get the total fluorescent densities for each case. The ratio $\eta_{fCal}/\eta_f(t)$ was then found to give R_t for that particular laser intensity.

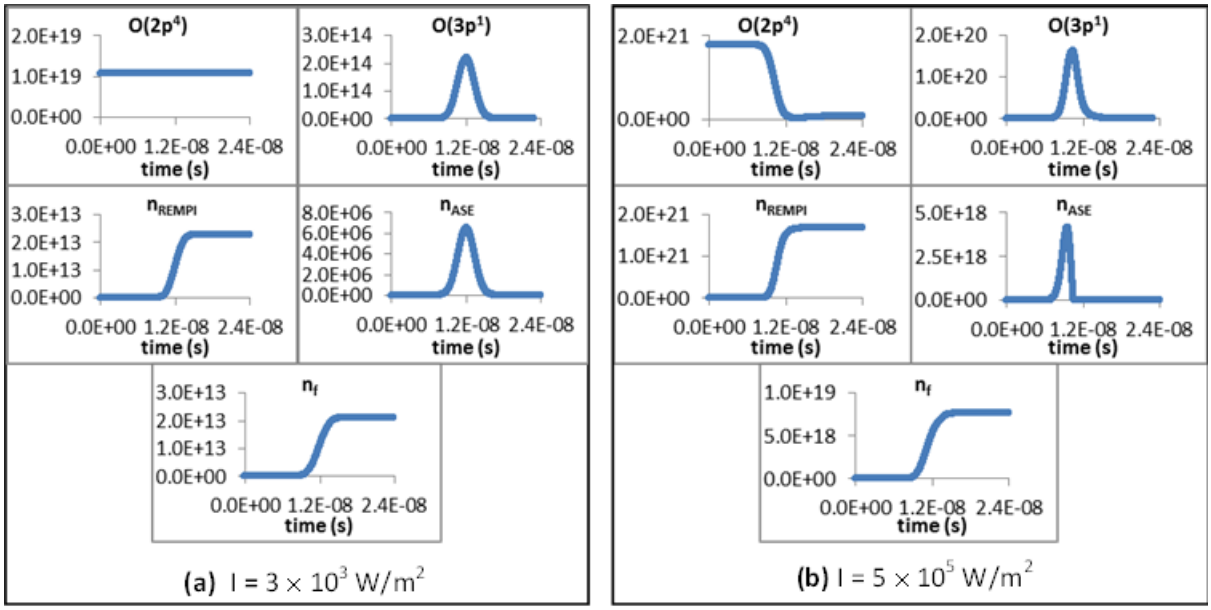

Figure 2A: Simulation results for O(2p^4), O(3p^1), REMPI, TALISE and fluorescent photon density n_f obtained using the model for (a) laser intensities of 3×10^3 W/m^2. (b) laser intensities of 5×10^5 W/m^2. ASE refers to TALISE in these figures.

AC stark effects were not included in the model as the threshold intensity for this effect is ~ 4×10^{13} W/m^2 and our model was only applied for intensities of 3×10^6 W/m^2 or lower, which is significantly lower than the threshold value [27]. The simulations were run over a laser intensity range of 1×10^2 W/m^2 - 3×10^6 W/m^2. The resulting R_t values are shown in figure 5. For low laser intensities the fluorescence has quadratic laser power dependence. In this region R_t has a value of 2 and shows no variation with laser intensity or pulse width. As the intensity increases the R_t values begin to decrease as ground state depletion becomes significant. With very large ground state depletion (> 98 %) R_t increases with increasing laser intensity as TALISE and REMPI densities get larger and dominate the TALIF photon densities.
Sample model results are included in figure 2A which show densities for the main species of interest at laser intensities of 3×10^3 W/m^2 and 5×10^5 W/m^2 respectively. At a laser intensity of 3×10^3

W/m^2 the graphs show that saturation effects are very weak. There is no noticeable ground state depletion and the fluorescent photon density is not dominated by REMPI or TALISE. In this regime TALIF exhibits quadratic laser power dependence and R_t has a value of 2. At a laser intensity of 5×10^5 W/m^2 saturation effects are significantly larger and can be clearly seen in the graphs. Ground state depletion is ~ 98% and REMPI and TALISE densities are equivalent to or dominate the fluorescent density. The laser power dependence is no longer quadratic and the R_t value deviates from 2 depending on the laser intensity. For the laser intensity range used in the model to generate the R_t values shown in figure 5, an error analysis showed an uncertainty ~ 5×10^{-5} in the R_t values.

References

[1] Kong M G, Kroesen G, Morfill G, Nosenko T, Shimizu T,van Dijk J, and Zimmermann J L 2009 *New J. Phys.* **11** 115012.
[2] Fridman G, Friedman G, Gutsol A, Shekhter A B, Vasilets V N and Fridman A 2008 Applied plasma medicine *Plasma Process. Polym.* **5** 503–33.
[3] Stoffels E, Kieft I E, Sladek R E J, van den Bedem L J M, van der Laan E P and Steinbuch M 2006 *Plasma Sources Sci. Technol.* **15** S169–80.
[4] Joeng J Y, Babayan S E, Tu V J, Park J, Henins I, Hicks R F and Selwyn G S 1998 *Plasma Sources Sci. Technol.* **7** 282–5.
[5] Nowling G R, Babayan S E, Jankovic V and Hicks R F 2002 *Plasma Sources Sci. Technol.* **11** 97–103.
[6] Knake N, Reuter S, Niemi K, Schulz von-der Gathen V, and Winter J 2008 *J. Phys. D: Appl. Phys.* 41 194006.
[7] van Gessel A F H, Grootel S C and Bruggeman P J 2013 *Plasma Sources Sci. Technol.* **22** 055010.
[8] Reuter R, Rügner K, Ellerweg D, de los Arcos T, von Keudell A and Benedikt J 2012 *Plasma Process. Polym.* **9** 1116–24
[9] Collart E J H, Baggerman J A G and Visser R J 1995 *J. Appl. Phys.* **78** 47.
[10] Carr E C, Ellis K A and Buhrman R A 1995 *Appl. Phys. Lett.* **66** (12) 1492.
[11] Niemi K, Schulz-Von der Gathen V and Döbele H F 2005 *Plasma Sources Sci. Technol.* **14** 375.
[12] Jiang C and Carter C 2014 *Plasma Sources Sci. Technol.* **23** 65006.
[13] Zhang S, Sobota A, van Veldhuizen E M and Bruggeman P J 2015 *Plasma Sources Sci. Technol.* **24** 045015.
[14] Van Gaens W, Bruggeman P J and Bogaerts A 2014 *New J. Phys.* 16 063054.
[15] Zhang S, van Gessel A F H, van Grootel S C and Bruggeman 2014 P J *Plasma Sources Sci. Technol.* **23** 025012
[16] Reuter S, Niemi K, Schulz-von der Gathen V and Döbele H F 2009 *Plasma Sources Sci. Technol.* **18** 015006
[17] Conway J, Kechkar S, O'Connor N, Gaman C, Turner M M and Daniels S 2013 *Plasma Sources Sci. Technol.* **22** 045004.
[18] Döbele H F, Mosbach T, Neimi K and Schultz-von der Gathen V 2005 *Plasma Sources Sci. Technol.* **14** S31
[19] Niemi K, O'Connell D, de Oliveira N, Joyeux D, Nahon L, Booth J P and Ganz T 2014 *Appl. Phys. Lett.* **103** 034102.
[20] Amorim J, Baravian G and Jolly J 2000 *J. Phys. D: Appl. Phys.* 33 R51.
[21] Goehlich A, Kawetzki T and Döbele H F 1998 *J. Chem. Phys.* **108** 9362.
[22] Schmidt J B, Sands B L, Kulatilaka W D, Roy S, Scofield J and Gord J R 2015 *Plasma Sources Sci. Technol.* **24** 032004.
[23] Kulatilaka W D, Gord J R, Katta V R, and Roy S 2012 Opt. Lett. **37** 3051.
[24] Kulatilaka W D, Roy S , Jiang N and Gord J R 2016 Appl. Phys. B **122** 1.
[25] Booth J P, Azamoum Y, Sirse N and Chabert P 2012 *J. Phys. D: Appl. Phys.* **45** 195201.
[26] Ono K, Oomori T, Tuda M and Namba K 1992 *J. Vac. Sci.Technol.* A **10** 1071.
[27] Huang Y and Gordon R 1992 *J. Chem. Phys* **97** 6363.
[28] Gogna G S, Kelly S and Daniels S 2015 32nd ICPIG Romania.
[29] Saxon R and Eichler J 1986 *Phys. Rev.* A **34** 199.
[30] Hasson V and Nicholls R W 1971 *J. Phys. B* **4** 1789.
[31] Stancu G D, Kaddouri F, Lacoste D A and Laux C O 2010 *J. Phys. D: Appl. Phys.* **43** 124002

[32] Van Gessel B, Brandenburg R and Bruggemann P 2013 *Appl. Phys. Lett.* **103** 064103.
[33] Liu L, Zhang J and Wang D 2009 *Plasma Sci. Technol.* 11 693
[34] Riley M E 1990 *Phys. Rev. A* **41** 4843.
[35] Dixit N, Levin D A and McKoy B V 1988 *Phys. Rev. A* **37** 4220.